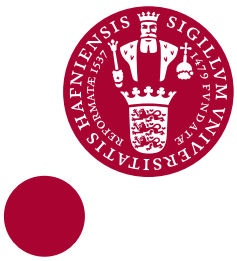

Genetic and structural insights into broad neutralization of hepatitis C virus by human VH1-69 antibodies

Tzarum, Netanel; Giang, Erick; Kong, Leopold; He, Linling; Prentoe, Jannick; Augestad, Elias; Hua, Yuanzi; Castillo, Shaun; Lauer, Georg M.; Bukh, Jens; Zhu, Jiang; Wilson, Ian A.; Law, Mansun

Published in:
Science Advances

DOI:
10.1126/sciadv.aav1882

Publication date:
2019

Document version
Publisher's PDF, also known as Version of record

VIROLOGY

Genetic and structural insights into broad neutralization of hepatitis C virus by human V_H1-69 antibodies

Netanel Tzarum[1], Erick Giang[2], Leopold Kong[1], Linling He[2], Jannick Prentoe[3], Elias Augestad[3], Yuanzi Hua[1], Shaun Castillo[2], Georg M. Lauer[4], Jens Bukh[3], Jiang Zhu[1,2]*, Ian A. Wilson[1,5]*, Mansun Law[2]*

An effective vaccine to the antigenically diverse hepatitis C virus (HCV) must target conserved immune epitopes. Here, we investigate cross-neutralization of HCV genotypes by broadly neutralizing antibodies (bNAbs) encoded by the relatively abundant human gene family *V_H1-69*. We have deciphered the molecular requirements for cross-neutralization by this unique class of human antibodies from crystal structures of HCV E2 in complex with bNAbs. An unusually high binding affinity is found for germ line–reverted versions of V_H1-69 precursor antibodies, and neutralization breadth is acquired during affinity maturation. Deep sequencing analysis of an HCV-immune B cell repertoire further demonstrates the importance of the *V_H1-69* gene family in the generation of HCV bNAbs. This study therefore provides critical insights into immune recognition of HCV with important implications for rational vaccine design.

INTRODUCTION

A prophylactic vaccine will be crucial for controlling the worldwide hepatitis C virus (HCV) epidemic. HCV infects an estimated 1 to 2% of the world population, leading to 400,000 deaths annually (*1*), and is a major cause of liver failure and hepatocellular carcinoma. Recent advances have been made in the treatment of patients with persistent HCV infection using direct-acting antiviral (DAA) therapies (*2*, *3*). However, an effective HCV vaccine is still much needed because of the increase in new infections and the poor awareness of carriers, especially in developing countries and among marginalized populations (*4*, *5*). Despite successful DAA treatment, patients with advanced liver disease remain at risk of liver cancer (*6*–*8*).

A major roadblock for HCV vaccine development is the genetic diversity of HCV, as demonstrated by 7 major HCV genotypes and more than 80 subtypes (*9*, *10*). Therefore, an effective vaccine must induce robust immune responses against a wide spectrum of HCV variants. The E2 envelope glycoprotein mediates viral entry by binding the CD81 receptor and other host factors (*11*–*13*). The receptor binding site on E2 is likely surface exposed and structurally conserved, thereby presenting a highly desirable target for broadly neutralizing antibodies (bNAbs) known as the neutralizing face of E2. Similar to the HIV-1 envelope glycoprotein, HCV E2 is extensively covered by N-linked glycans (*14*) and has several variable regions (VRs), particularly hypervariable region 1 (HVR1), which shield conserved epitopes and assist in viral escape from NAbs (Fig. 1A) (*9*, *15*).

Previously, we isolated a panel of human monoclonal Abs (mAbs) that recognize five distinct antigenic regions (ARs; AR1–5) on the HCV E1E2 glycoprotein complex (*16*, *17*). While mAbs targeting AR1 and AR2 showed limited neutralizing activity, mAbs recognizing AR3 (AR3A–D) exhibit cross-genotype neutralization and inhibition of CD81 receptor binding to E1E2 (*16*, *17*). The heavy chains (HCs) of AR3A–D share a similar genetic background and are derived from Ab precursors of the *V_H1-69* gene family that have been reported to be associated with cross-neutralization of HCV (*16*–*19*), influenza virus (*20*–*24*), and HIV-1 (*25*). Recently, two independent studies reported bNAbs isolated from patients that spontaneously cleared HCV and are also derived from *V_H1-69* genes and target AR3 (*26*, *27*). These findings underscore the role of human V_H1-69 Abs in combatting HCV infections and highlight the potential benefits of eliciting V_H1-69–derived bNAbs by vaccination.

RESULTS

Here, we investigate how V_H1-69 bNAbs achieve cross-genotype recognition of the E2 neutralizing face and the genetic requirements for the immune system to generate such bNAbs. To overcome the inherent flexibility of E2 (*28*), we designed an E2 core domain construct (*29*) of the prototypic genotype 1a isolate, H77, and determined its crystal structure with bNAb AR3C (Fig. 1B and fig. S1A) (*29*). In parallel, Khan *et al.* (*30*) reported the crystal structure of a different E2 core construct derived from a genotype 2a isolate, J6, with nonneutralizing mAb 2A12. Structural analysis of H77 E2c in complex with AR3C Fab and alanine scanning mutagenesis (*16*, *29*, *31*) mapped AR3 to the E2 front layer and part of the CD81 binding loop (amino acids 426 to 443 and 529 to 531; Fig. 1A and fig. S1). Most residues in AR3 are highly conserved among HCV genotypes (fig. S1C and table S1). Negative-stain electron microscopy revealed that in soluble E2, AR3 is exposed on the surface and not masked by the glycan shield or by VRs 1 to 3 (VR1–3; Fig. 1B) (*29*). To examine the accessibility of the AR3 neutralizing epitopes in soluble E2, we investigated binding of four AR3-directed mAbs

[1]Department of Integrative Structural and Computational Biology, The Scripps Research Institute, La Jolla, CA 92037, USA. [2]Department of Immunology and Microbiology, The Scripps Research Institute, La Jolla, CA 92037, USA. [3]Copenhagen Hepatitis C Program (CO-HEP), Department of Infectious Diseases, Hvidovre Hospital, and Department of Immunology and Microbiology, Faculty of Health and Medical Sciences, University of Copenhagen, Copenhagen, Denmark. [4]Gastrointestinal Unit and Liver Center, Massachusetts General Hospital and Harvard Medical School, Boston, MA 02114, USA. [5]Skaggs Institute for Chemical Biology, The Scripps Research Institute, La Jolla, CA 92037, USA.
*Corresponding author. Email: mlaw@scripps.edu (M.L.); wilson@scripps.edu (I.A.W.); jiang@scripps.edu (J.Z.)

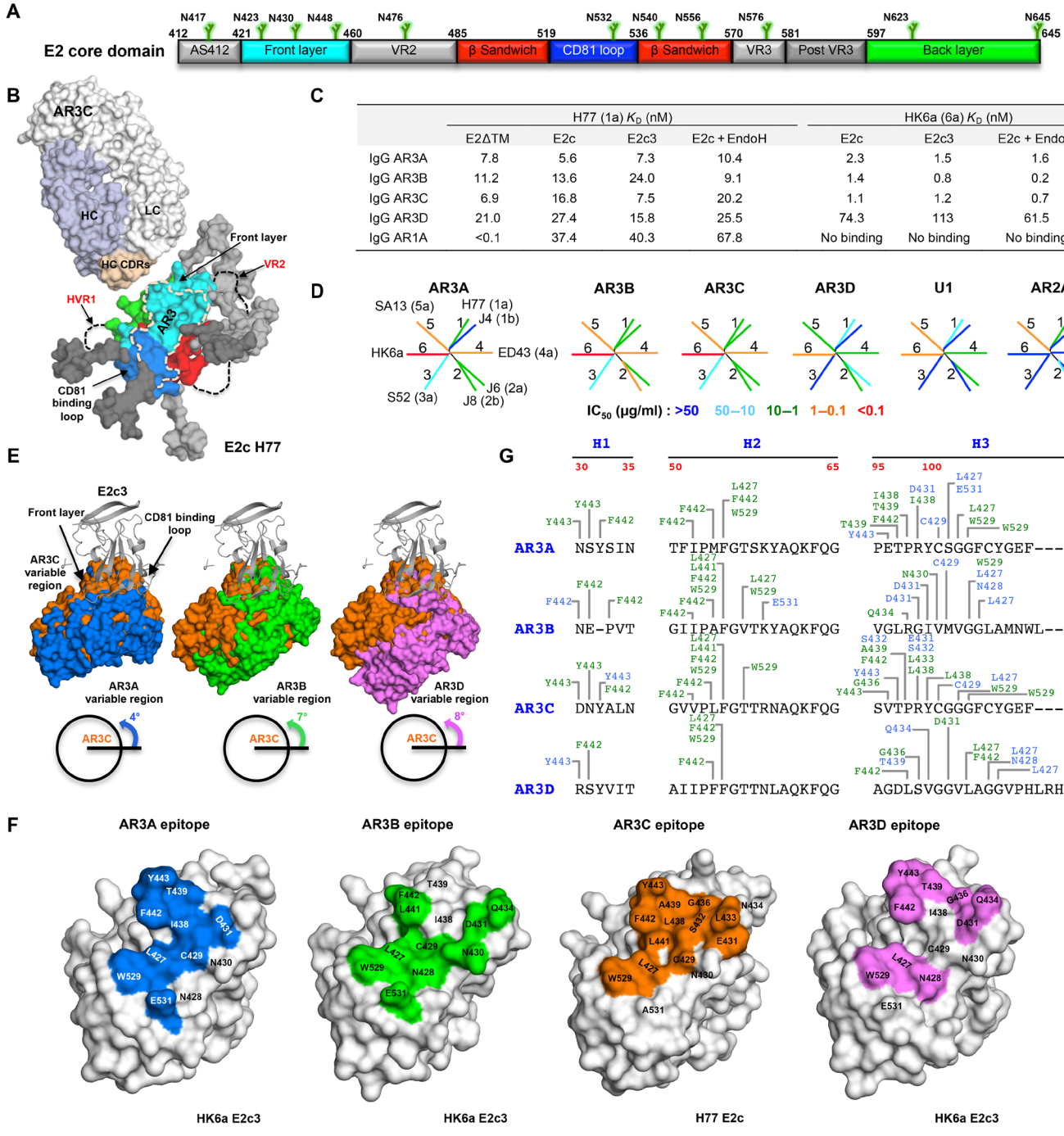

	H77 (1a) K_D (nM)				HK6a (6a) K_D (nM)		
	E2ΔTM	E2c	E2c3	E2c + EndoH	E2c	E2c3	E2c + EndoH
IgG AR3A	7.8	5.6	7.3	10.4	2.3	1.5	1.6
IgG AR3B	11.2	13.6	24.0	9.1	1.4	0.8	0.2
IgG AR3C	6.9	16.8	7.5	20.2	1.1	1.2	0.7
IgG AR3D	21.0	27.4	15.8	25.5	74.3	113	61.5
IgG AR1A	<0.1	37.4	40.3	67.8	No binding	No binding	No binding

Fig. 1. Crystal structures of HK6a E2c3 and AR3 Fab complexes. (**A**) Schematic representations of the E2 core domain (amino acids 412 to 645) colored by structural components, with VRs in gray, front layer in cyan, β sandwich in red, CD81 loop in blue, and back layer in green. The E2 HVR1, stalk, and transmembrane region (amino acids 384 to 410 and 646 to 746) are not shown. The E2 N-linked glycans are indicated (*29*). (**B**) Modeling of the HVR1, VR2, and the $Man_6GlcNac_2$ N-linked glycans in the complex structure of H77 E2c, indicating the accessibility of AR3. The $Man_6GlcNac_2$ N-linked glycans were modeled on the basis of the N430 glycan in the H77 E2c structure [Protein Data Bank (PDB) entry 4MWF]. The AR3 is marked by a dashed line. The glycans that surround the AR3 are colored in dark gray. (**C**) K_D values of various AR3 immunoglobulin G (IgG) binding to E2ΔTM, E2c, and E2c3 from genotypes 1a and 6a. (**D**) Neutralization breadth of AR3A–D, U1, and AR2A mAbs tested by HCVcc assays. Dendrograms shown for each mAb are colored on the basis of their half maximal inhibitory concentration (IC_{50}) values. (**E**) Superposition of the crystal structures of HK6a E2c3-AR3A (blue), -AR3B (green), or -AR3D (pink) complexes with H77 E2c-AR3C (orange) illustrating the differences in the angle of approach of the AR3A–D mAbs to E2c. The structures of the HK6a E2c3-AR3A, -AR3B, or -AR3D complexes were superimposed with H77 E2c-AR3C on the basis of E2, and for each complex, the angle between the Cα atoms of HC V111, HC F54, and light chain (LC) I106 was calculated. The angle of approach was determined as the relative change in the angle between AR3A, AR3B, and AR3D mAbs to AR3C. For clarity, only the Fab VRs and the HK6a E2c3 structure are shown. (**F**) AR3 epitopes. The E2c structures are shown in surface representation, and the interacting residues in the epitopes were colored and labeled. (**G**) Schematic overview of the interactions between E2 and the AR3 HCs. The CDR sequences are aligned, and E2 interacting residues are highlighted in blue (hydrogen bonds) and green (hydrophobic interactions).

AR3A–D to genotype 1a H77 E2 ectodomain (E2ΔTM), E2c, and E2c3 [E2c with VR3 deleted (*28*)] (fig. S2A). Nanomolar binding (K_D) for all three E2 constructs indicates that mAb recognition of AR3 is not dependent on the VRs (Fig. 1C and fig. S2B), whereas a notable reduction was observed in AR1A binding to E2c and E2c3 (Fig. 1C and fig. S2B) (*16*). Modeling of $Man_6GlcNac_2$ N-linked glycans onto the E2 glycosylation sites reveals that AR3 itself is devoid of glycans, although encircled by three glycans (N423, N430, and N532; Fig. 1, A and B, and fig. S1B). Removal of the E2c glycans by Endoglycosidase H (EndoH) treatment had negligible effect on bNAb binding, confirming that the glycans are not essential for high binding affinity of the AR3 mAbs and, in soluble E2, the AR3 epitopes are not shielded by glycans (Fig. 1C and fig. S2B). In contrast, AR1A binding was reduced by EndoH treatment, suggesting that the glycans are essential for AR1A binding (Fig. 1C and fig. S2B).

Having established AR3 as a key site for HCV neutralization, we extended our structural efforts here to E2c constructs derived from other genotypes (see fig. S3A). The AR3A–D mAbs have cross-genotype binding activity (fig. S3B) that can be used to study the neutralizing face of E2. In addition, AR3A–C mAbs exhibited neutralization breadth among genotypes 1 to 6 strains, whereas AR3D had a more restricted breadth in virus neutralization assays (Fig. 1D and fig. S3C). Crystallization trials of E2c from different genotypes with AR3A–D Fabs resulted in diffraction-quality crystals for E2c3 of the HK6a isolate as complexes with AR3A, AR3B, and AR3D (table S2 and see also Materials and methods). The HK6a E1E2 glycoprotein complex has been shown to be fully functional in vitro [HCV pseudotype particle (HCVpp) and cell culture HCV (HCVcc) systems] and in vivo (chimpanzee and human liver chimeric mouse models). The HK6a E2c3 structures (fig. S4A) revealed that the overall fold is similar to genotypes 1a H77 E2c (*29*) and 2a J6 E2 core (*30*), with Cα root mean square deviations of 1.09 and 0.86 Å, respectively (for amino acids 491 to 645, using E2c3 from the AR3A complex as representative of the HK6a E2 structures). However, substantial conformational differences were observed in the β sandwich loop connecting β6 and β7 (amino acids 540 to 552; fig. S4B) in the VR3 region (fig. S4C) and in the N-terminal part of the back layer (amino acids 564 to 610). Less pronounced differences were seen in the C-terminal part of the back layer (amino acids 629 to 640) and AR3C epitope of H77 E2 (AR3 is absent in the J6 structure; fig. S4B). The β6-β7 loop of HK6a shows a different conformation compared to H77 and J6, which could result from an N540E substitution that eliminates the seventh N-glycosylation site (N540) that is present in genotypes 1, 2, 4, and 5 but not in genotypes 3 and 6 (figs. S3A and S4, D and E).

Superposition of four E2-AR3 Fab complexes indicates that these Abs bind AR3 with different angles of approach (Fig. 1E) and with their footprints mapped to different but overlapping parts of the antigenic surface (Fig. 1F), consistent with our previous biophysical study indicating flexibility of the E2 front layer and CD81 binding loop (*28*) (fig. S4F). Analysis of the interactions between the AR3 Fabs and HK6a E2c3, compared to AR3C and H77 E2c (Fig. 1G and fig. S4G), indicates that E2 recognition is mediated mainly by their HCs (*29*) with few interactions with the LCs. The interaction between HC complementarity-determining regions (CDRs) 1 and 2 with AR3 mainly involves hydrophobic and aromatic side chains, whereas CDRH3 also makes a large number (5 to 8) of main chain—main chain hydrogen bonds with E2 (Fig. 1G and table S3).

It has been shown that V_H1-69–derived bNAbs against influenza virus and HIV-1 interact with conserved hydrophobic residues in their antigens via hydrophobic residues at the tip of their CDRH2 loops (*20*–*25*). Sequence alignment of the *V_H1-69*–encoded AR3 mAb HCs indicates a relatively low identity (62 to 73%) for the V_H region (amino acids 1 to 110; fig. S5A) and even less for the CDR loops (35 to 57%), especially CDRH3 (Fig. 1G). Nevertheless, the CDRH2 tip of AR3A–D mAbs still retains a hydrophobic motif of I/V52-P52a-X53-F54 (X = hydrophobic residue; Fig. 2A), which makes hydrophobic contacts with a highly conserved hydrophobic pocket between the front layer and CD81 binding loop, despite some variations in CDRH2 interactions. The AR3 mAbs have longer than average CDRH3 loops (18 to 22 residues) that interact with a flexible region of the front layer (amino acids 430 to 437; Fig. 1G). Their CDRH3 adopts a β hairpin stabilized by intra-CDR hydrogen bonds and further enhanced by a disulfide between the CDRH3 β strands in AR3A and AR3C (fig. S5B). The β hairpin conformations vary depending on CDRH3 length, but the two glycines at its apex contact L427 and W529 (for AR3A–C) of E2 (fig. S5B). Buried surface area (BSA) analysis confirms the indispensable role of the HC (Fig. 2B and fig. S5C). The HC BSA is similar for AR3A, AR3C, and AR3D (648 to 683 $Å^2$), but slightly greater for AR3B (797 $Å^2$). Structural analysis suggests that the optimal CDRH3 length for the AR3-like bNAbs is 18 to 22 residues, because a shorter loop will likely generate steric clashes with E2, especially with glycans surrounding AR3 (fig. S5D); a longer loop would result in E2 being further away (Fig. 2C), causing a reduction in binding and neutralization breadth, as observed for AR3D mAb (Fig. 1, C and D).

Therefore, we further characterized Abs from an HCV-immune Ab library (*16*, *17*). Within 22 E1E2 HC binding groups, 7 were encoded by the *V_H1-69* germline (GL) gene with CDRH3 loops ranging from 12 to 22 residues (fig. S5E). Abs from groups B (including AR1A) and E have shorter CDRH3s (15 or 12 residues, respectively) and little neutralization activity (*16*). Notably, CDRH2 of AR1A no longer contains the I/V52-P52a-X53-F54 hydrophobic motif (Fig. 2A). Fabs from group U also target AR3 (*17*), with a similar CDRH2 hydrophobic motif but a 17-residue CDRH3 (Fig. 2A and fig. S5F); mAb U1 however had limited neutralization breadth (Fig. 1D). A similar reduction was observed when CDRH3 of AR3A was shortened by 1 residue to 17 residues (fig. S5G). Together, the results suggest that a hydrophobic CDRH2 tip and CDRH3 length of 18 to 22 residues capable of forming main-chain hydrogen bonds with the E2 front layer are optimal for broad neutralization by AR3 mAbs (Fig. 2D).

In the HIV field, it is widely acknowledged that maturation of bNAbs from their GL Ab precursors is a long evolutionary process (>2 to 5 years) involving selection for mutations contributing to B cell survival and improved Ab functions. Therefore, an in-depth analysis of how GL precursors recognize their target antigen can provide critical insights into bNAb induction (*32*). The IMGT V-QUEST program (*33*) was used to predict GL genes for HC (V_H, D_H, and J_H) and LC (V_L and J_L) of AR3A–D mAbs (fig. S6A). The inferred GL precursors (AR3A–D_{GL}) and variants with only the V_H gene reverted (AR3A–D_{1-69}) were synthesized. In comparison with anti-HIV bNAbs, AR3 mAbs exhibit relatively low levels of somatic hypermutation (SHM), with identity to the V_H GL of 84 to 91% and 74 to 84% at the nucleotide and amino acid levels, respectively (Fig. 3A and fig. S6B), similar to that of V_H1-69 anti-influenza bNAbs (*23*). Although CDRH2 contains a number of mutations

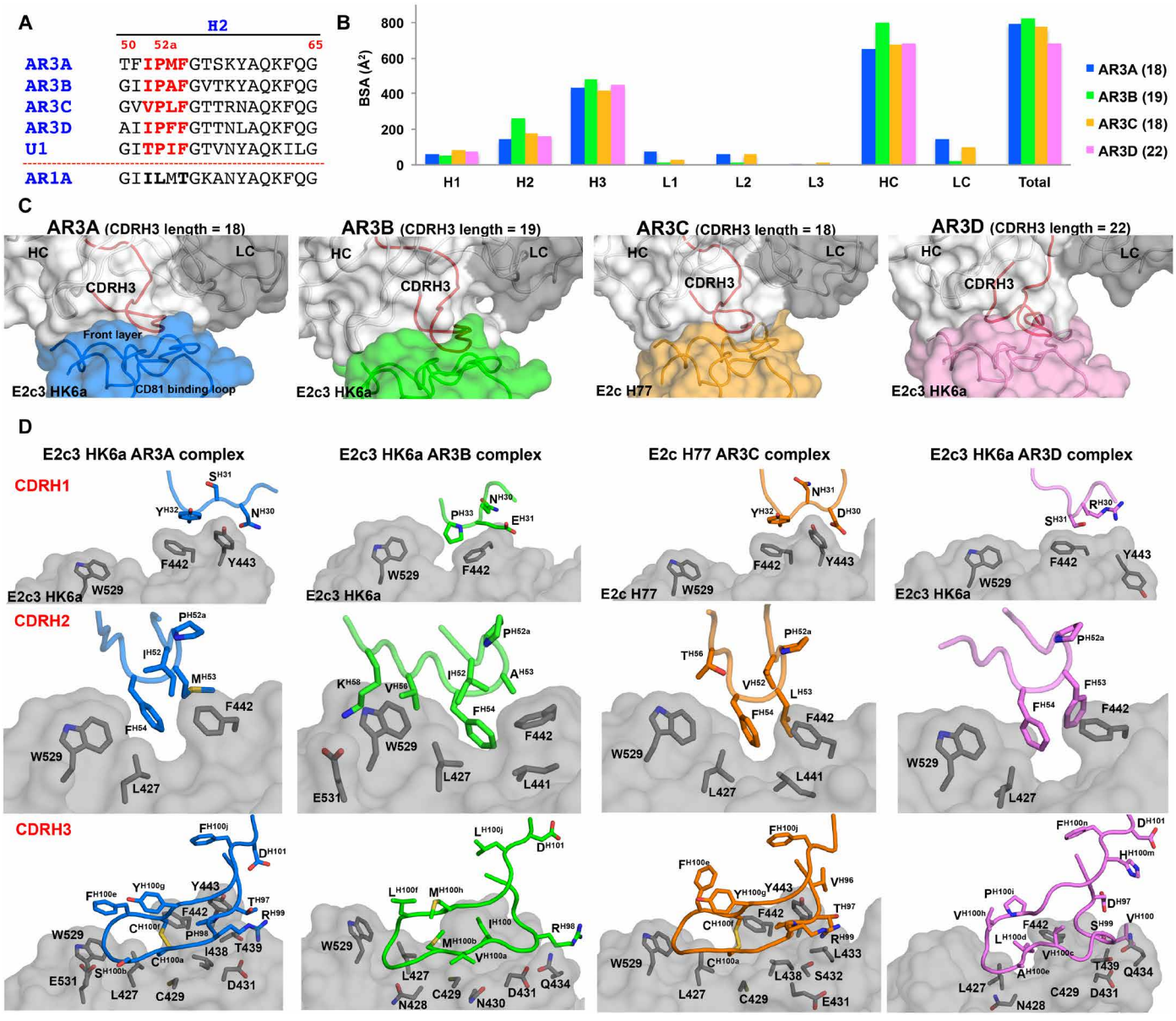

Fig. 2. Features that enable broad neutralization by AR3 mAbs. (**A**) Alignment of the CDRH2 sequences of AR3 bNAbs and mAbs U1 and AR1A. The hydrophobic motif in CDRH2 is highlighted in red. (**B**) Surface area buried by the CDRs of AR3 mAbs on E2s. CDRH3 length is indicated in brackets. (**C**) Correlation between CDRH3 length and LC surface area buried. CDRH3 is colored in red. (**D**) Interactions between E2 and CDRH1-3 of AR3A–D.

(amino acid identity of 64 to 76% with GL), the CDRH2 hydrophobic motif that presumably initiates the interaction with the E2 hydrophobic pocket is conserved from the GL (Fig. 3A). Binding of $AR3_{GL}$ and $AR3_{1-69}$ IgGs by enzyme-linked immunosorbent assay (ELISA) reveals that $AR3A_{1-69}$, $AR3B_{1-69}$, and $AR3C_{GL}$ interact with both H77 E2c and HK6a E2c (fig. S6C). Further quantification using biolayer interferometry for these GL precursors indicated only a 2- to 8-fold decrease in K_D for H77 and 22- to 120-fold for HK6a (Fig. 3B and fig. S6D). AR3A–D_{GL} and AR3A–D_{1-69} (*34*) exhibited some neutralization above the 50% level for $AR3A_{1-69}$, $AR3A_{GL}$, and $AR3B_{1-69}$, and more weakly for $AR3C_{1-69}$ and $AR3C_{GL}$, mainly against genotypes 5a and 6a (Fig. 3C), suggesting that neutralization breadth was acquired during affinity maturation. Thus, HCV binding and neutralization can be readily detected in V_H1-69 precursors.

Our GL reversion analysis and other studies (*17*, *18*, *26*) highlight the important role of the *V_H1-69* gene family in E2 recognition and in broad neutralizing responses against HCV. Since the AR3 mAbs were isolated from an HCV-immune phage display Ab library, we used next-generation sequencing (NGS) to characterize enrichment of AR3-like mAbs during panning. The original and three other libraries from panning against native and epitope-masked E1E2 were subjected to NGS, followed by antibodyomics analysis (table S4 and see also Materials and methods). Quantitative library profiles show distinct patterns indicative of rapid enrichment after three panning steps (Pan1 to Pan3) using E1E2 (Fig. 4A). V_H1 is predominantly

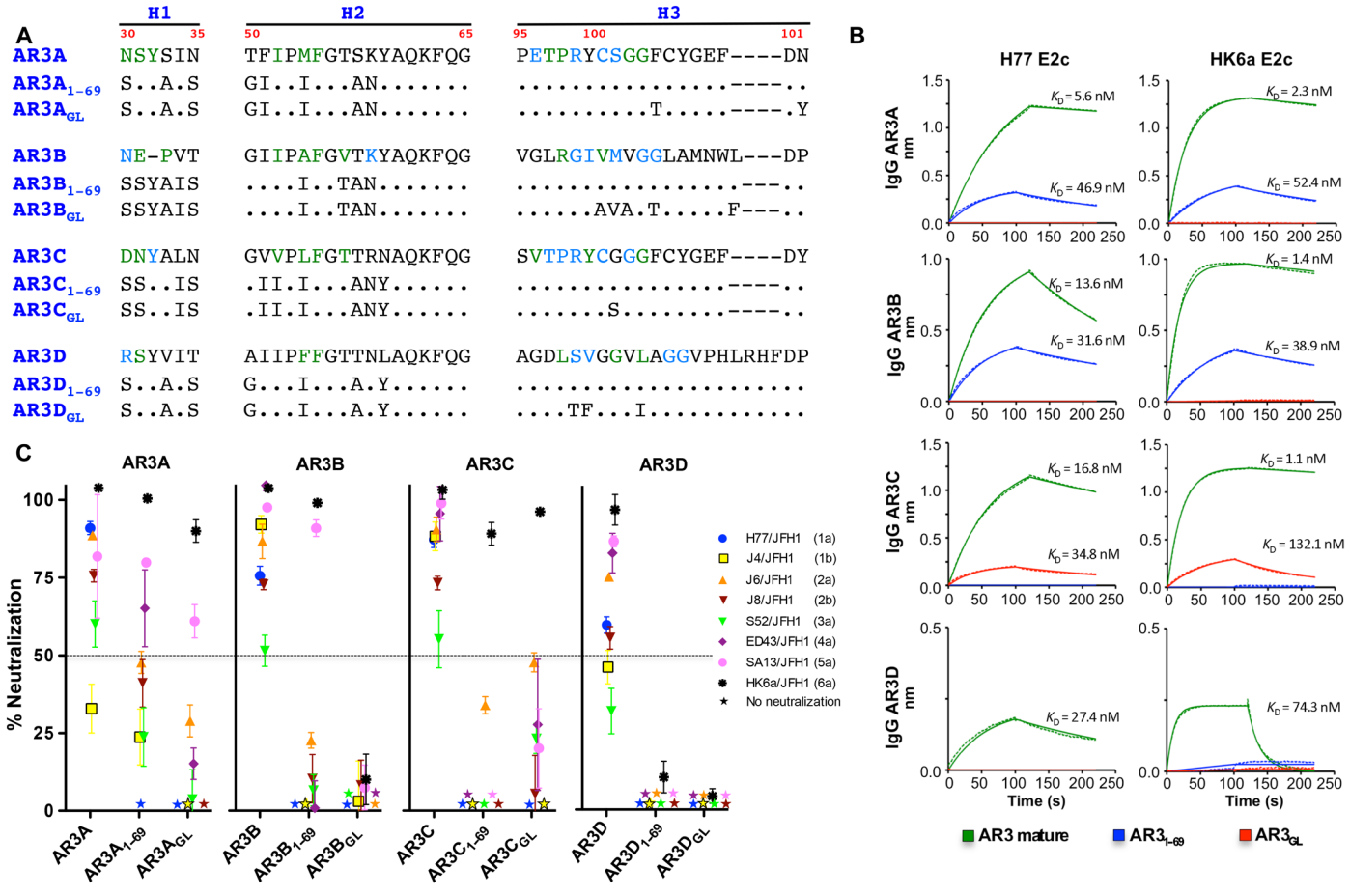

Fig. 3. The inferred GL of AR3 mAbs. (**A**) Alignment of the HC CDRs of AR3, $AR3_{GL}$ (inferred GL), and $AR3_{1–69}$ (reversion of only the V_H gene to the V_H1-69 sequence). The interacting residues in the mature mAbs are colored in blue (hydrogen bonds) and green (hydrophobic interactions). (**B**) Biolayer interferometry analysis of $AR3_{1–69}$ and $AR3_{GL}$ IgGs binding to H77 and HK6a E2c. (**C**) Single-dose (50 μg/ml) neutralization assay of $AR3_{1–69}$ and $AR3_{GL}$ IgGs against the eight HCVcc JFH1-based Core-NS2 recombinants of genotypes 1 to 6. Error bars represent SEM.

selected in the converged Fab library, with V_H1-69 accounting for 87% of the total V_H population. A notable shift was observed in SHM, with the peak value increasing from 7–9% to 15–16% in Pan3 (Fig. 4A), and CDRH3 length also increased from 10 to 14 residues to enrichment of 15 to 17 residues (Fig. 4A). Two-dimensional (2D) identity/divergence plots visualize enrichment of AR1–3 mAbs from this Fab library (Fig. 4B and fig. S7A) by showing sequences with CDRH3 identity of 85% or higher (orange dots with number and library percentage labeled). Using AR3C as an example, the 2D plot shows a slow but steady increase of AR3C-like HCs from 0.01% in the prepanning library to 0.5% in the third panning cycle. Similar trends were observed for other AR3 mAbs with long CDRH3s (fig. S7A). By comparison, AR1A shows rapid convergence during antigen selection with a 14,500-fold increase (0.004 to 58%), consistent with the dominant peak of 15-residue CDRH3s (Fig. 4, A and B). In our analysis, HCs with similar CDRH3 loops and low levels of SHM (0 to 10%) that represent intermediate Abs in the library were also identified (Fig. 4B, marked by rectangles, and fig. S7). This provides useful clues as to how these Abs evolved to acquire E1E2 specificity and affinity.

To assess the prevalence of V_H1-69 AR3 mAbs in comparison to those targeting other E1E2 antigenic sites, we also sequenced the Fab libraries panned with an E1E2 antigen that was masked with AR1 and AR3 Abs (*17*). HCV-specific mAbs of other GL origins were selected, including the V_H1-18, V_H3-30, and V_H5-51 families, some of which are cross-NAbs that recognize AR4 and AR5 on the quaternary E1E2 complex. Other mAb groups include mAbs that bind to epitopes that overlap with AR4 and AR5 (mAbs from groups R1 and S1) and non–cross-NAbs that bind to epitopes overlapping with AR1–3 [groups F, I, K, M, and T; for more details, see (*17*)]. Quantitative library profiles displayed little change in V_H gene usage, SHM, and CDRH3 length during this epitope-masked panning (fig. S7B), confirming that mAbs AR4A and AR5A, although present in the prepanning library, were only slightly enriched during selection (fig. S7C). Thus, NGS analysis of an HCV-immune Fab library following antigen challenge revealed the prevalence of V_H1-69–derived Abs targeting AR1 and AR3 of E2, whereas Abs of other GL origins recognize different E1E2 antigenic sites (Fig. 4C).

To investigate whether this V_H1-69 preference is indeed common to HCV-specific bNAbs, we sequenced Ab repertoires of five patients with chronic HCV and compared their repertoires with those from high levels of anti-E1E2 Ab titers and cross-neutralizing activity and compared their repertoires with those from five healthy individuals as controls. Overall, both repertoires displayed similar V_H gene distributions, with three subjects in each group showing relatively high

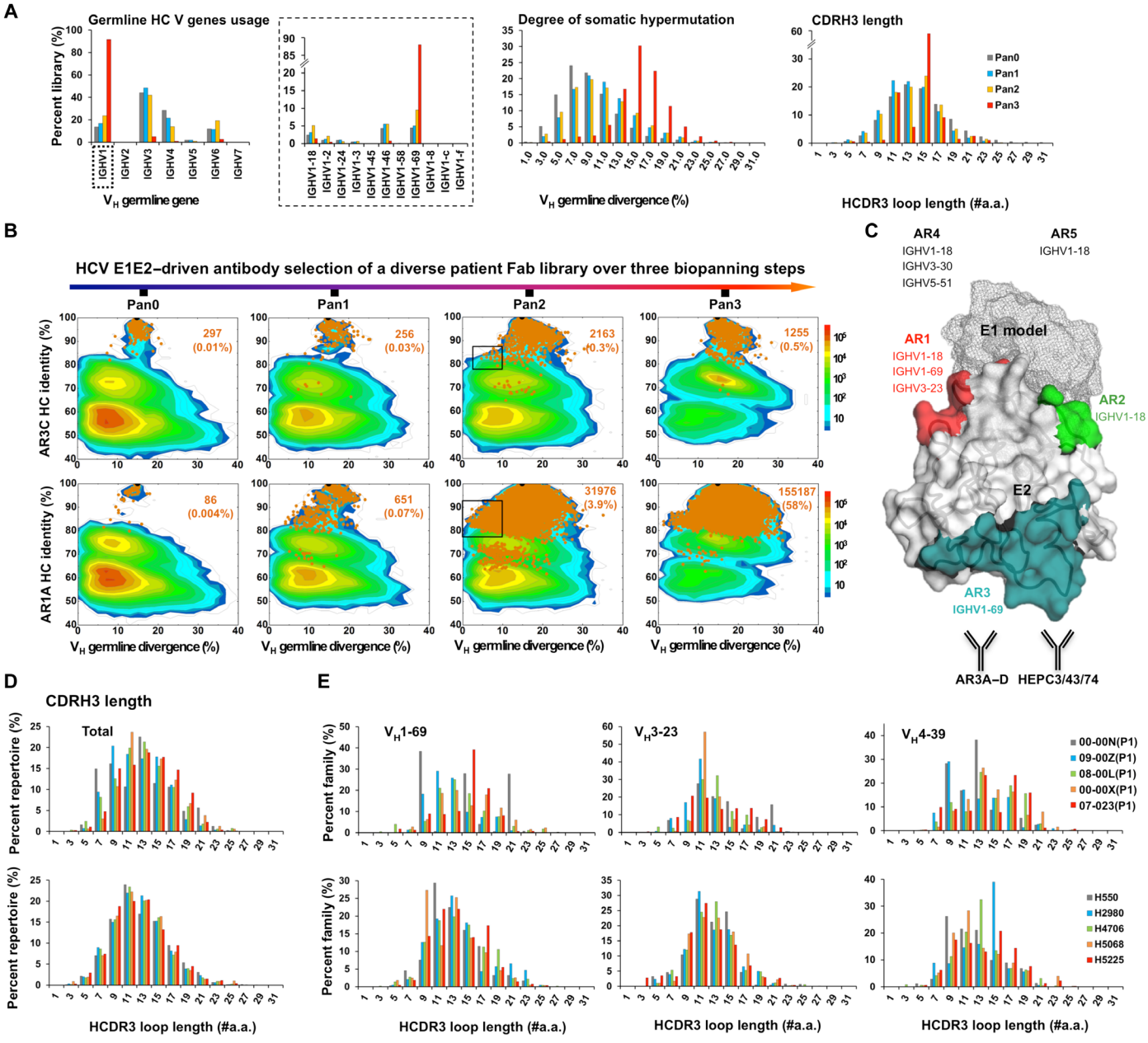

Fig. 4. Analysis of B cell repertoires of HCV-infected donors. (**A**) Quantitative B cell repertoire distribution of HC GL V gene usage, degree of SHM, and CDRH3 length and (**B**) identity/divergence analysis (to AR mAb/V_H GL) of the prepanned and panned phage display Ab libraries. #a.a., number of amino acids. The panning experiments were performed using E1E2. (**C**) Schematic representation of the epitopes and the HC variable genes encoding the AR1–5 mAbs. The AR1–3 epitopes are shown on the E2 structure (*16*, *17*, *31*). bNAbs that target the AR3 epitopes are listed. (**D**) The distribution of CDRH3 length in the total HC GL V genes and (**E**) the three largest HC GL gene families of five patients with chronic HCV with high anti-E1E2 Ab titers and cross-neutralizing activity (top) and five healthy donors (bottom) as controls.

frequencies of V_H1-69 (fig. S8A). The HCV-infected donor repertoires exhibit a slightly broader range of CDRH3 lengths than the uninfected controls [normal distribution peaking around 11 to 14 residues (Fig. 4D)], yet with no significant difference for the average length of the HCDR3 loop between the two groups (fig. S10). Further analysis of the three largest V_H gene families suggests that the distribution of some gene families could be affected by HCV infection (Fig. 4E). In contrast, both HCV-infected and healthy donors exhibit normal CDRH3 length distributions for the *V_H3-23* gene family. Some differences are also observed for other GL gene families (fig. S8B). Comparing the SHM between the two groups indicates similar distribution of both the HC and LC (fig. S8C). Comparison of the average SHM for the *V_H1-69* gene family and for the overall V_H repertoire indicates no significant difference between the two groups (fig. S10), although the sample size here is too small for conclusive statistical analysis.

DISCUSSION

The Centers for Disease Control and Prevention recently reported an almost threefold increase in the number of new HCV infections

in the United States between 2010 and 2015 (*35*), a result of the increase in injection drug users caused by the opioid crisis in America (*36*), underscoring the urgent need for an effective HCV vaccine. The extreme genetic diversity of HCV demands elicitation of cross-genotype immune responses from vaccination. Therefore, structural understanding of bNAb recognition, together with the knowledge on how bNAbs develop from their GL precursors, is essential for the rational design of HCV vaccine immunogens (*32*, *37*). As a main target for bNAbs, AR3 is highly conserved and overlaps with the majority of the E2 neutralizing face (*29*, *38*). It was previously shown that, on native virions, HCV neutralization epitopes are shielded by HVR1 (*9*, *15*) and glycans (*39*). To overcome the HCV escape by shielding of neutralization epitopes, it is crucial to design an antigen that can elicit a high level of bNAbs to conserved epitopes. Our results indicate that AR3 bNAb recognition of soluble E2 is largely independent of VRs (HVR1, VR2, and VR3) or glycans, highlighting that the AR3 and the neutralizing face are promising targets for inclusion in an HCV vaccine, although a better understanding of the entire E1E2 complex would likely serve to optimize this further.

The E2c structures with bNAbs AR3A–D suggest that flexibility of the front layer facilitates binding of bNAbs encoded by the *V_H1-69* GL gene family. Other critical features for breadth of AR3-like bNAbs include a hydrophobic CDRH2 tip and CDRH3 of around 18 to 22 residues. The absence of one or more of these features can result in reduced neutralization breadth (as suggested for mAb U1; Fig. 1D). In contrast to HIV-1 (*32*), some AR3 inferred GL mAbs bind E2 with high affinity, and low to medium SHM is sufficient to neutralize virus, although further somatic mutation can improve breadth. Our results are consistent with a recent study (*27*), in which AR3-like bNAbs of *V_H1-69* origin and with similar SHM were isolated from patients with spontaneous viral clearance, suggesting that HCV bNAbs can achieve broad neutralization with rapid lineage development. A possible reason is that the hydrophobic CDRH2 motif that interacts with critical E2 residues for CD81 binding is GL encoded. The tip of the CDRH2 encoded by the *V_H1-69* gene is the most hydrophobic among the human HC genes (*25*) and therefore has superiority for targeting the hydrophobic E2 neutralizing face and hydrophobic pockets in the flu hemagglutinin stem region (*22*, *23*). Since most of the interactions of CDRH3 with E2 are main chain—main chain hydrogen bonds, they can tolerate variation in the sequence of the CDRH3 and, therefore, low levels of SHM can be sufficient to optimize the interaction with E2.

While HCV-directed bNAbs can stem from different GL genes, bNAbs encoded by *V_H1-69* have been reported in multiple studies (*16*, *18*, *26*, *27*), suggesting an important role of this Ab family in the immune response to HCV. Our analysis revealed that V_H1-69 Abs target AR1 and AR3 on E2 when HCV E1E2 was the panning antigen, but significant enrichment of AR1 non-NAbs suggests that AR1 may be more accessible in this format. However, other GL gene families are also involved in host Ab response to HCV. For rational vaccine design, a preferable strategy would appear to be developing HCV antigens that present the conserved AR3 neutralizing epitopes to engage the *V_H1-69* gene family, which is one of the frequent Ab families in the human Ab repertoire. It was recently reported that naïve B cells with high-avidity GL-encoded B cell receptors produce mainly IgM^+ memory B cells following immunization in mice (*40*). If this is also true in humans, then one may expect that a GL-targeting strategy and E2-based vaccine antigens will trigger the generation of mostly antiviral V_H1-69 IgM^+ memory B cells. Such a strategy should be taken into consideration in HCV vaccine studies. Furthermore, HCV appears to be an excellent model for studying host humoral immunity to viral infection.

MATERIALS AND METHODS

Expression and purification of the soluble E2 from genotypes 1 to 6

The DNA constructs of the prototypic isolate H77 (*41*) for E2c (truncation of N and C termini and VR2 and removal of N448 and N576 glycosylation sites) and E2c3 (additional removal of VR3) were engineered on the basis of the soluble E2 ectodomain (E2ΔTM, amino acids 384 to 717) as previously described (*28*, *29*). On the basis of sequence similarity to H77, E2c constructs of HCV1 (*42*), CON1 (*43*), UKN1b12.6 (*44*), J6 (*45*), UKN3A1.28c (*44*), S52 (*46*), ED43 (*47*), SA13 (*48*), and HK6a (*34*) isolates and the E2c3 constructs of H77, ED43, and HK6a isolates were engineered and synthesized by GeneArt (Invitrogen, USA; fig. S3A). Notably, the E1E2 envelope glycoprotein complex of the HK6a isolate was previously shown to be fully functional in vitro using the HCVpp and HCVcc systems and in vivo in chimpanzee and human liver chimeric mouse models (*34*, *49*, *50*). The E2 constructs were expressed and purified as previously described (*29*).

Expression and purification of the AR3 IgGs and Fabs

IgGs AR1A, AR3A, AR3B, AR3C, AR3D, and U1 were expressed and purified as previously described (*16*). The AR3A–D_{GL} and AR3A–$D_{1–69}$ variable domain genes were synthesized by GeneArt (Invitrogen, USA), cloned into the pIgG vector, and expressed as previously described (*16*). Fabs AR3C and AR3D were cloned into the phagemid vector pComb3H and transformed into the BL21 (DE3) bacterial strain (Novagen) for expression in the presence of IPTG (isopropyl-β-D-thiogalactopyranoside) overnight at 16°C. The bacterial cells were treated with lysozyme, sonicated, and the Fabs were purified on a protein G affinity column. Fabs AR3A and AR3B were generated from the corresponding IgGs (*16*) by papain digestion (Sigma-Aldrich). All Fabs were further purified by size exclusion chromatography using a Superdex 200 column (Pharmacia) in 50 mM NaCl, 20 mM tris-HCl (pH 7.2) buffer.

Crystallization and structural determination of E2c3 HK6a-Fab complexes

From the 10 HCV isolates, only 4 isolates [H77 (1a), J6 (2a), ED43 (4a), and HK6a (6a)] gave high yield and were therefore used for the structural studies. The E2-Fab AR3 complexes were formed by overnight incubation of purified E2 and each AR3 Fab in a molar ratio of 1:1.25 (E2:Fab) at room temperature, followed by size exclusion chromatography (Superdex 200) to remove unbound Fab using 20 mM tris and 50 mM NaCl (pH 7.2) buffer. Crystallization experiments were performed using the vapor diffusion sitting drop method at 20°C. Crystallization experiments of the E2c from the H77, J6, ED43, and HK6a isolates in complex with AR3A–D yielded no crystals. However, further engineering the E2c proteins (E2c3; fig. S2A) resulted in crystals of the HK6a isolate in complexes with AR3A–D (table S2) that diffracted to 2.80, 2.60, and 3.30 Å for the AR3A, AR3B, and AR3D complexes, respectively, and to low resolution (~10 Å) for AR3C complexes. Crystals of the E2c3 HK6a-Fab AR3A complex were obtained using a reservoir solution of 20% (w/v) PEG 3500, 0.2 M sodium citrate (pH 8.2); crystals of E2c3

HK6a-Fab AR3B complex from a reservoir solution of 20% (w/v) PEG 3500, 0.2 M Li chloride (pH 6.7); and crystals of E2c3 HK6a-Fab AR3D complex from a reservoir solution of 20% (w/v) PEG 6000, 0.1 M Hepes (pH 7.0). Prior to data collection, all crystals were cryoprotected with 10% ethylene glycol and flash cooled in liquid nitrogen. Diffraction datasets were collected at the Advanced Photon Source (APS) and the Stanford Synchrotron Radiation Lightsource (SSRL) (table S2). Data were integrated and scaled using HKL2000 (*51*). The E2c3 HK6a-Fab AR3A structure was solved by molecular replacement method using Phaser (*52*), with the E2c H77-Fab AR3C (PDB entry 4MWF) as a search model. The E2c3 HK6a-Fab AR3B and E2c3 HK6a-Fab AR3D structures were solved by molecular replacement method using the refined E2c3 HK6a-Fab AR3A structure as a search model. Structure refinement was carried out in Phenix (*53*), and model building was performed with COOT (*54*). Final refinement statistics are summarized in table S2.

Enzyme-linked immunosorbent assay

Purified E2 isolates were coated onto microwells at 5 μg/ml overnight at 4°C. After blocking with 4% (w/v) nonfat dry milk in dilution buffer (PBS + 0.02% Tween 20) for 30 min, titrated AR3 Abs (purified Ab for fig. S3B and transfected supernatant of Abs from 293T cells for fig. S6C) in dilution buffer with 1% nonfat dry milk were added to the microwells and incubated for 1 hour at room temperature. Titrated Abs were detected with secondary Ab horseradish peroxidase–conjugated goat anti-human IgG Fc (Jackson ImmunoResearch) and developed with 3,3′,5,5′-tetramethylbenzidine substrate (Thermo Fisher Pierce). The reaction was stopped with 2 N sulfuric acid, and developed plates were read at absorbance of 450 nm.

K_D determination

K_D values were determined by biolayer interferometry using an Octet RED instrument (ForteBio Inc.). IgGs at ~10 μg/ml in a kinetics buffer [1× PBS (pH 7.4), 0.01% BSA, and 0.002% Tween 20] were immobilized onto protein G–coated biosensors and incubated with varying concentrations of E2 protein. The k_{on} and k_{off} values of each E2 protein for each IgG were measured in real time to determine K_D values. All binding data were collected at 30°C.

Neutralization assay

In vitro neutralization was carried on Huh7.5 cells using either a single high dose (50 μg/ml) or a dilution series of the relevant Ab as previously described (*55*). Control Ab b6 at the highest dose did not inhibit the viruses. For the dilution series experiments, IC_{50} values were calculated in GraphPad Prism 6 using a three-parameter curve fitting.

Panning of the phage display library

The construction of the phage display Ab library was previously described (*16*, *17*). In summary, RNA of mononuclear cells from the bone marrow of a patient with chronic HCV was extracted, and complementary DNA (cDNA) was synthesized. LC and HC fragments were amplified using gene-specific primers and cloned into phagemid vector with randomized HC and LC pairing. For antigen panning, the Ab Fab fragments were expressed as a fusion protein to the phage coat protein III for surface display. The HCV-immune phage display Ab library was panned for three consecutive rounds with increasing washing stringency in two different panning experiments (*16*, *17*). In the first experiment, recombinant E1E2 proteins captured by *Galanthus nivalis* lectin were used as the panning antigens. In the second experiment, E1E2 antigens captured by mAb AR3A and blocked with mAb AR1B were used (*17*). In each panning step, antigen was directly coated onto a microtiter plate, followed by blocking with 4% (w/v) milk in PBS. The phage library was added to the wells and incubated for 1 to 2 hours at 37°C, and unbound phages were washed away with PBS/0.5% (v/v) Tween 20. Bound phages were eluted and used to infect freshly grown *Escherichia coli* (XL1-Blue, Stratagene) for titration on LB agar plates with carbenicillin.

Clinical samples

Normal blood donor samples were procured from the Normal Blood Donor Service (NBDS) of The Scripps Research Institute (TSRI). All healthy donors tested negative for hepatitis B virus, HCV, and HIV (*56*). Blood samples from patients with HCV with long-term chronic HCV viremia (genotype 1 or genotype 3) were collected at Massachusetts General Hospital. Informed consent was given by all subjects under a protocol approved by the Partners Human Research Committee [Institutional Review Board (IRB) no. 1999P004983]. Peripheral blood mononuclear cells (PBMCs) were extracted by Ficoll-Paque (GE Healthcare Life Sciences) density gradient centrifugation. Plasma samples were evaluated for E1E2-specific Ab by ELISA and for virus neutralizing activity using HCVpp (*17*). Five HCV^+ donor samples with high cross-neutralizing activity and five random normal blood donor samples were selected for sequencing analysis below.

NGS and bioinformatics analysis

NGS was performed on the Ion Torrent Personal Genome Machine (PGM) and S5 systems. The HC regions of the Fab phage libraries were amplified from the plasmid stock using PCR with vector-specific primers (tables S4 and S5 and fig. S9). Notably, the forward primer contained a PGM/S5 full-length P1 adaptor, whereas the reverse primer contained a PGM/S5 A adaptor and an Ion Xpress barcode (Life Technologies) to differentiate Fab phage libraries. A total of 25 PCR cycles were performed, and the PCR products with an expected length of 500 to 600 bp were gel purified (Qiagen). The resulting HC libraries were quantitated using the Qubit 2.0 Fluorometer with the Qubit dsDNA HS Assay Kit. The dilution factor required for PGM template preparation was determined such that the final concentration was 50 pM. For the prepanning Fab library (Pan0), template preparation was performed with the Ion PGM Template IA 500 Kit, followed by NGS on the Ion PGM system using the Ion PGM Hi-Q Sequencing Kit and an Ion 316 v2 chip. For the postpanning libraries (Pan1 to Pan3) obtained from two E1E2 panning procedures, template preparation and (Ion 530) chip loading were performed on Ion Chef using the Ion 530 Ext Kit, followed by NGS on the Ion S5 System. For five normal donors and five HCV-infected donors studied here, a previously reported 5′-RACE (rapid amplification of cDNA ends) PCR protocol was used to capture their B cell repertoires in an unbiased manner (table S4) (*57*). Briefly, total RNA was extracted from 5 to 10 million PBMCs into 30 μl of water with the RNeasy Mini Kit (Qiagen). 5′-RACE was performed with the SMARTer RACE cDNA Amplification Kit (Clontech). The Ig PCRs were set up with the Platinum Taq High-Fidelity DNA Polymerase (Life Technologies) in a total volume of 50 μl, with 5 μl of cDNA as template, 1 μl of 5′-RACE primer, and 1 μl

of 10 μM reverse primer. The 5′-RACE primer contained a PGM/S5 P1 adaptor, whereas the reverse primer contained a PGM/S5 A adaptor and an Ion Xpress barcode (Life Technologies) to differentiate donor libraries. A similar PCR protocol (25 cycles) was used, and the PCR products with an expected length of 600 bp were gel purified (Qiagen). The Ab HC and LC (κ and λ) libraries were quantitated using the Qubit 2.0 Fluorometer with the Qubit dsDNA HS Assay Kit and mixed at a ratio of 1:1:1 for each donor. The five donor libraries were further mixed at an equal ratio for template preparation and (Ion 530) chip loading on Ion Chef using the Ion 530 Ext Kit. NGS was performed on the Ion S5 System with default settings. The human antibodyomics pipeline (*57*–*63*) was used to process and annotate the NGS data of Fab libraries and Ab repertoires. Notably, a number of methodological modifications have been made to the pipeline to improve data quality (*64*).

SUPPLEMENTARY MATERIALS

Supplementary material for this article is available at http://advances.sciencemag.org/cgi/content/full/5/1/eaav1882/DC1

Fig. S1. AR3 epitopes.
Fig. S2. Binding of AR3A–D and AR1A IgGs to E2.
Fig. S3. Binding and neutralization of AR3 mAbs to HCV isolates from genotypes 1 to 6.
Fig. S4. Crystal structures of HK6a E2c3 with AR3 Fabs.
Fig. S5. Features that enable broad neutralization by AR3.
Fig. S6. The inferred GL genes of the AR3 mAbs.
Fig. S7. Identity/divergence analysis of the phage display library from an HCV-infected donor.
Fig. S8. B cell repertoire of healthy and HCV-infected donors.
Fig. S9. Primers that were used for amplification of the HC regions of the Fab phage libraries in the different panning steps.
Fig. S10. Summary of the statistic analysis of the NGS of HCV chronically infected and healthy donors.
Table S1. Amino acid sequence variation of the E2 protein of HCV genotypes 1 to 7.
Table S2. Data collection and refinement statistics for HK6a E2c3 AR3 Fab complex structures.
Table S3. Hydrogen bond and hydrophobic interactions between E2 and the HC of AR3 Fabs.
Table S4. NGS of HCV-immune Ab repertoire of an HCV-infected patient.
Table S5. NGS of HCV-immune Ab repertoires.
References (*65*–*68*)

REFERENCES AND NOTES

1. Global hepatitis report (2017); www.who.int/hepatitis/publications/global-hepatitis-report2017/en/.
2. E. R. Feeney, R. T. Chung, Antiviral treatment of hepatitis C. *BMJ* **348**, g3308 (2014).
3. J.-M. Pawlotsky, J. J. Feld, S. Zeuzem, J. H. Hoofnagle, From non-A, non-B hepatitis to hepatitis C virus cure. *J. Hepatol.* **62**, S87–S99 (2015).
4. G. L. Armstrong, A. Wasley, E. P. Simard, G. M. McQuillan, W. L. Kuhnert, M. J. Alter, The prevalence of hepatitis C virus infection in the United States, 1999 through 2002. *Ann. Intern. Med.* **144**, 705–714 (2006).
5. M. Thursz, A. Fontanet, HCV transmission in industrialized countries and resource-constrained areas. *Nat. Rev. Gastroenterol. Hepatol.* **11**, 28–35 (2014).
6. F. Conti, F. Buonfiglioli, A. Scuteri, C. Crespi, L. Bolondi, P. Caraceni, F. G. Foschi, M. Lenzi, G. Mazzella, G. Verucchi, P. Andreone, S. Brillanti, Early occurrence and recurrence of hepatocellular carcinoma in HCV-related cirrhosis treated with direct-acting antivirals. *J. Hepatol.* **65**, 727–733 (2016).
7. M. A. Konerman, A. S. F. Lok, Hepatitis C treatment and barriers to eradication. *Clin. Transl. Gastroenterol.* **7**, e193 (2016).
8. S. Pol, Lack of evidence of an effect of direct-acting antivirals on the recurrence of hepatocellular carcinoma: Data from three ANRS cohorts. *J. Hepatol.* **65**, 734–740 (2016).
9. J. Prentoe, R. Velázquez-Moctezuma, S. K. H. Foung, M. Law, J. Bukh, Hypervariable region 1 shielding of hepatitis C virus is a main contributor to genotypic differences in neutralization sensitivity. *Hepatology* **64**, 1881–1892 (2016).
10. D. B. Smith, P. Becher, J. Bukh, E. A. Gould, G. Meyers, T. Monath, A. S. Muerhoff, A. Pletnev, R. Rico-Hesse, J. T. Stapleton, P. Simmonds, Proposed update to the taxonomy of the genera *Hepacivirus* and *Pegivirus* within the *Flaviviridae* family. *J. Gen. Virol.* **97**, 2894–2907 (2016).
11. B. D. Lindenbach, C. M. Rice, The ins and outs of hepatitis C virus entry and assembly. *Nat. Rev. Microbiol.* **11**, 688–700 (2013).
12. M. B. Zeisel, D. J. Felmlee, T. F. Baumert, Hepatitis C virus entry. *Curr. Top. Microbiol. Immunol.* **369**, 87–112 (2013).
13. L. Fénéant, S. Levy, L. Cocquerel, CD81 and hepatitis C virus (HCV) infection. *Viruses* **6**, 535–572 (2014).
14. A. Goffard, J. Dubuisson, Glycosylation of hepatitis C virus envelope proteins. *Biochimie* **85**, 295–301 (2003).
15. J. Prentoe, L. Verhoye, R. Velázquez Moctezuma, C. Buysschaert, A. Farhoudi, R. Wang, H. Alter, P. Meuleman, J. Bukh, HVR1-mediated antibody evasion of highly infectious in vivo adapted HCV in humanised mice. *Gut* **65**, 1988–1997 (2016).
16. M. Law, T. Maruyama, J. Lewis, E. Giang, A. W. Tarr, Z. Stamataki, P. Gastaminza, F. V. Chisari, I. M. Jones, R. I. Fox, J. K. Ball, J. A. McKeating, N. M. Kneteman, D. R. Burton, Broadly neutralizing antibodies protect against hepatitis C virus quasispecies challenge. *Nat. Med.* **14**, 25–27 (2008).
17. E. Giang, M. Dorner, J. C. Prentoe, M. Dreux, M. J. Evans, J. Bukh, C. M. Rice, A. Ploss, D. R. Burton, M. Law, Human broadly neutralizing antibodies to the envelope glycoprotein complex of hepatitis C virus. *Proc. Natl. Acad. Sci. U.S.A.* **109**, 6205–6210 (2012).
18. C. H. Chan, K. G. Hadlock, S. K. H. Foung, S. Levy, *V_H1-69* gene is preferentially used by hepatitis C virus-associated B cell lymphomas and by normal B cells responding to the E2 viral antigen. *Blood* **97**, 1023–1026 (2001).
19. Z.-Y. Keck, J. Xia, Y. Wang, W. Wang, T. Krey, J. Prentoe, T. Carlsen, A. Y.-J. Li, A. H. Patel, S. M. Lemon, J. Bukh, F. A. Rey, S. K. H. Foung, Human monoclonal antibodies to a novel cluster of conformational epitopes on HCV E2 with resistance to neutralization escape in a genotype 2a isolate. *PLOS Pathog.* **8**, e1002653 (2012).
20. C. Dreyfus, N. S. Laursen, T. Kwaks, D. Zuijdgeest, R. Khayat, D. C. Ekiert, J. H. Lee, Z. Metlagel, M. V. Bujny, M. Jongeneelen, R. van der Vlugt, M. Lamrani, H. J. W. M. Korse, E. Geelen, Ö. Sahin, M. Sieuwerts, J. P. J. Brakenhoff, R. Vogels, O. T. W. Li, L. L. M. Poon, M. Peiris, W. Koudstaal, A. B. Ward, I. A. Wilson, J. Goudsmit, R. H. E. Friesen, Highly conserved protective epitopes on influenza B viruses. *Science* **337**, 1343–1348 (2012).
21. D. C. Ekiert, G. Bhabha, M.-A. Elsliger, R. H. E. Friesen, M. Jongeneelen, M. Throsby, J. Goudsmit, I. A. Wilson, Antibody recognition of a highly conserved influenza virus epitope. *Science* **324**, 246–251 (2009).
22. S. Lang, J. Xie, X. Zhu, N. C. Wu, R. A. Lerner, I. A. Wilson, Antibody 27F3 broadly targets influenza A group 1 and 2 hemagglutinins through a further variation in V_H1-69 antibody orientation on the HA stem. *Cell Rep.* **20**, 2935–2943 (2017).
23. L. Pappas, M. Foglierini, L. Piccoli, N. L. Kallewaard, F. Turrini, C. Silacci, B. Fernandez-Rodriguez, G. Agatic, I. Giacchetto-Sasselli, G. Pellicciotta, F. Sallusto, Q. Zhu, E. Vicenzi, D. Corti, A. Lanzavecchia, Rapid development of broadly influenza neutralizing antibodies through redundant mutations. *Nature* **516**, 418–422 (2014).
24. J. Sui, W. C. Hwang, S. Perez, G. Wei, D. Aird, L.-M. Chen, E. Santelli, B. Stec, G. Cadwell, M. Ali, H. Wan, A. Murakami, A. Yammanuru, T. Han, N. J. Cox, L. A. Bankston, R. O. Donis, R. C. Liddington, W. A. Marasco, Structural and functional bases for broad-spectrum neutralization of avian and human influenza A viruses. *Nat. Struct. Mol. Biol.* **16**, 265–273 (2009).
25. C.-C. Huang, M. Venturi, S. Majeed, M. J. Moore, S. Phogat, M.-Y. Zhang, D. S. Dimitrov, W. A. Hendrickson, J. Robinson, J. Sodroski, R. Wyatt, H. Choe, M. Farzan, P. D. Kwong, Structural basis of tyrosine sulfation and V_H-gene usage in antibodies that recognize the HIV type 1 coreceptor-binding site on gp120. *Proc. Natl. Acad. Sci. U.S.A.* **101**, 2706–2711 (2004).
26. S. J. Merat, R. Molenkamp, K. Wagner, S. M. Koekkoek, D. van de Berg, E. Yasuda, M. Böhne, Y. B. Claassen, B. P. Grady, M. Prins, A. Q. Bakker, M. D. de Jong, H. Spits, J. Schinkel, T. Beaumont, Hepatitis C virus broadly neutralizing monoclonal antibodies isolated 25 years after spontaneous clearance. *PLOS ONE* **11**, e0165047 (2016).
27. J. R. Bailey, A. I. Flyak, V. J. Cohen, H. Li, L. N. Wasilewski, A. E. Snider, S. Wang, G. H. Learn, N. Kose, L. Loerinc, R. Lampley, A. L. Cox, J. M. Pfaff, B. J. Doranz, G. M. Shaw, S. C. Ray, J. E. Crowe Jr., Broadly neutralizing antibodies with few somatic mutations and hepatitis C virus clearance. *JCI Insight* **2**, e92872 (2017).
28. L. Kong, D. E. Lee, R. U. Kadam, T. Liu, E. Giang, T. Nieusma, F. Garces, N. Tzarum, V. L. Woods Jr., A. B. Ward, S. Li, I. A. Wilson, M. Law, Structural flexibility at a major conserved antibody target on hepatitis C virus E2 antigen. *Proc. Natl. Acad. Sci. U.S.A.* **113**, 12768–12773 (2016).
29. L. Kong, E. Giang, T. Nieusma, R. U. Kadam, K. E. Cogburn, Y. Hua, X. Dai, R. L. Stanfield, D. R. Burton, A. B. Ward, I. A. Wilson, M. Law, Hepatitis C virus E2 envelope glycoprotein core structure. *Science* **342**, 1090–1094 (2013).
30. A. G. Khan, J. Whidby, M. T. Miller, H. Scarborough, A. V. Zatorski, A. Cygan, A. A. Price, S. A. Yost, C. D. Bohannon, J. Jacob, A. Grakoui, J. Marcotrigiano, Structure of the core ectodomain of the hepatitis C virus envelope glycoprotein 2. *Nature* **509**, 381–384 (2014).
31. R. Gopal, K. Jackson, N. Tzarum, L. Kong, A. Ettenger, J. Guest, J. M. Pfaff, T. Barnes, A. Honda, E. Giang, E. Davidson, I. A. Wilson, B. J. Doranz, M. Law, Probing the antigenicity of hepatitis C virus envelope glycoprotein complex by high-throughput mutagenesis. *PLOS Pathog.* **13**, e1006735 (2017).
32. D. R. Burton, L. Hangartner, Broadly neutralizing antibodies to HIV and their role in vaccine design. *Annu. Rev. Immunol.* **34**, 635–659 (2016).

33. M.-P. Lefranc, C. Pommié, M. Ruiz, V. Giudicelli, E. Foulquier, L. Truong, V. Thouvenin-Contet, G. Lefranc, IMGT unique numbering for immunoglobulin and T cell receptor variable domains and Ig superfamily V-like domains. *Dev. Comp. Immunol.* **27**, 55–77 (2003).
34. J. M. Gottwein, T. K. H. Scheel, T. B. Jensen, J. B. Lademann, J. C. Prentoe, M. L. Knudsen, A. M. Hoegh, J. Bukh, Development and characterization of hepatitis C virus genotype 1-7 cell culture systems: Role of CD81 and scavenger receptor class B type I and effect of antiviral drugs. *Hepatology* **49**, 364–377 (2009).
35. Surveillance for Viral Hepatitis – United States 2015 (2017); www.cdc.gov/hepatitis/statistics/2015surveillance/commentary.htm.
36. P. K. Muhuri, J. C. Gfroerer, M. C. Davies, *Associations of Nonmedical Pain Reliever Use and Initiation of Heroin Use in the United States* (Substance Abuse and Mental Health Services Administration, Center for Behavioral Health Statistics and Quality, 2013).
37. G. J. Nabel, Designing tomorrow's vaccines. *N. Engl. J. Med.* **368**, 551–560 (2013).
38. N. Tzarum, I. A. Wilson, M. Law, The neutralizing face of hepatitis C virus E2 envelope glycoprotein. *Front. Immunol.* **9**, 1315 (2018).
39. M. Lavie, X. Hanoulle, J. Dubuisson, Glycan shielding and modulation of hepatitis C virus neutralizing antibodies. *Front. Immunol.* **9**, 910 (2018).
40. K. A. Pape, R. W. Maul, T. Dileepan, A. S. Paustian, P. J. Gearhart, M. K. Jenkins, Naive B cells with high-avidity germline-encoded antigen receptors produce persistent IgM^+ and transient IgG^+ memory B cells. *Immunity* **48**, 1135–1143.e4 (2018).
41. A. A. Kolykhalov, E. V. Agapov, K. J. Blight, K. Mihalik, S. M. Feinstone, C. M. Rice, Transmission of hepatitis C by intrahepatic inoculation with transcribed RNA. *Science* **277**, 570–574 (1997).
42. Q. L. Choo, K. H. Richman, J. H. Han, K. Berger, C. Lee, C. Dong, C. Gallegos, D. Coit, R. Medina-Selby, P. J. Barr, Genetic organization and diversity of the hepatitis C virus. *Proc. Natl. Acad. Sci. U.S.A.* **88**, 2451–2455 (1991).
43. V. Lohmann, F. Körner, J.-O. Koch, U. Herian, L. Theilmann, R. Bartenschlager, Replication of subgenomic hepatitis C virus RNAs in a hepatoma cell line. *Science* **285**, 110–113 (1999).
44. D. Lavillette, A. W. Tarr, C. Voisset, P. Donot, B. Bartosch, C. Bain, A. H. Patel, J. Dubuisson, J. K. Ball, F.-L. Cosset, Characterization of host-range and cell entry properties of the major genotypes and subtypes of hepatitis C virus. *Hepatology* **41**, 265–274 (2005).
45. M. Yanagi, R. H. Purcell, S. U. Emerson, J. Bukh, Hepatitis C virus: An infectious molecular clone of a second major genotype (2a) and lack of viability of intertypic 1a and 2a chimeras. *Virology* **262**, 250–263 (1999).
46. J. M. Gottwein, T. K. H. Scheel, B. Callendret, Y.-P. Li, H. B. Eccleston, R. E. Engle, S. Govindarajan, W. Satterfield, R. H. Purcell, C. M. Walker, J. Bukh, Novel infectious cDNA clones of hepatitis C virus genotype 3a (strain S52) and 4a (strain ED43): Genetic analyses and in vivo pathogenesis studies. *J. Virol.* **84**, 5277–5293 (2010).
47. R. W. Chamberlain, N. Adams, A. A. Saeed, P. Simmonds, R. M. Elliott, Complete nucleotide sequence of a type 4 hepatitis C virus variant, the predominant genotype in the Middle East. *J. Gen. Virol.* **78**, 1341–1347 (1997).
48. J. Bukh, C. L. Apgar, R. Engle, S. Govindarajan, P. A. Hegerich, R. Tellier, D. C. Wong, R. Elkins, M. C. Kew, Experimental infection of chimpanzees with hepatitis C virus of genotype 5a: Genetic analysis of the virus and generation of a standardized challenge pool. *J. Infect. Dis.* **178**, 1193–1197 (1998).
49. J. Bukh, P. Meuleman, R. Tellier, R. E. Engle, S. M. Feinstone, G. Eder, W. C. Satterfield, S. Govindarajan, K. Krawczynski, R. H. Miller, G. Leroux-Roels, R. H. Purcell, Challenge pools of hepatitis C virus genotypes 1-6 prototype strains: Replication fitness and pathogenicity in chimpanzees and human liver-chimeric mouse models. *J. Infect. Dis.* **201**, 1381–1389 (2010).
50. J.-C. Meunier, R. E. Engle, K. Faulk, M. Zhao, B. Bartosch, H. Alter, S. U. Emerson, F.-L. Cosset, R. H. Purcell, J. Bukh, Evidence for cross-genotype neutralization of hepatitis C virus pseudo-particles and enhancement of infectivity by apolipoprotein C1. *Proc. Natl. Acad. Sci. U.S.A.* **102**, 4560–4565 (2005).
51. Z. Otwinowski, W. Minor, Processing of X-ray diffraction data collected in oscillation mode. *Methods Enzymol.* **276**, 307–326 (1997).
52. A. J. McCoy, R. W. Grosse-Kunstleve, L. C. Storoni, R. J. Read, Likelihood-enhanced fast translation functions. *Acta Crystallogr. D* **61**, 458–464 (2005).
53. P. D. Adams, R. W. Grosse-Kunstleve, L.-W. Hung, T. R. Ioerger, A. J. McCoy, N. W. Moriarty, R. J. Read, J. C. Sacchettini, N. K. Sauter, T. C. Terwilliger, PHENIX: Building new software for automated crystallographic structure determination. *Acta Crystallogr. D* **58**, 1948–1954 (2002).
54. P. Emsley, K. Cowtan, Coot: Model-building tools for molecular graphics. *Acta Crystallogr. D* **60**, 2126–2132 (2004).
55. R. Velázquez-Moctezuma, M. Law, J. Bukh, J. Prentoe, Applying antibody-sensitive hypervariable region 1-deleted hepatitis C virus to the study of escape pathways of neutralizing human monoclonal antibody AR5A. *PLOS Pathog.* **13**, e1006214 (2017).
56. J. E. Roughan, K. M. Reardon, K. E. Cogburn, H. Quendler, P. J. Pockros, M. Law, Chronic hepatitis C virus infection breaks tolerance and drives polyclonal expansion of autoreactive B cells. *Clin. Vaccine Immunol.* **19**, 1027–1037 (2012).
57. L. He, D. Sok, P. Azadnia, J. Hsueh, E. Landais, M. Simek, W. C. Koff, P. Poignard, D. R. Burton, J. Zhu, Toward a more accurate view of human B-cell repertoire by next-generation sequencing, unbiased repertoire capture and single-molecule barcoding. *Sci. Rep.* **4**, 6778 (2014).
58. L. Kong, B. Ju, Y. Chen, L. He, L. Ren, J. Liu, K. Hong, B. Su, Z. Wang, G. Ozorowski, X. Ji, Y. Hua, Y. Chen, M. C. Deller, Y. Hao, Y. Feng, F. Garces, R. Wilson, K. Dai, S. O'Dell, K. McKee, J. R. Mascola, A. B. Ward, R. T. Wyatt, Y. Li, I. A. Wilson, J. Zhu, Y. Shao, Key gp120 glycans pose roadblocks to the rapid development of VRC01-class antibodies in an HIV-1-infected Chinese donor. *Immunity* **44**, 939–950 (2016).
59. X. Wu, T. Zhou, J. Zhu, B. Zhang, I. Georgiev, C. Wang, X. Chen, N. S. Longo, M. Louder, K. McKee, S. O'Dell, S. Perfetto, S. D. Schmidt, W. Shi, L. Wu, Y. Yang, Z.-Y. Yang, Z. Yang, Z. Zhang, M. Bonsignori, J. A. Crump, S. H. Kapiga, N. E. Sam, B. F. Haynes, M. Simek, D. R. Burton, W. C. Koff, N. A. Doria-Rose, M. Connors; NISC Comparative Sequencing Program, J. C. Mullikin, G. J. Nabel, M. Roederer, L. Shapiro, P. D. Kwong, J. R. Mascola, Focused evolution of HIV-1 neutralizing antibodies revealed by structures and deep sequencing. *Science* **333**, 1593–1602 (2011).
60. T. Zhou, J. Zhu, X. Wu, S. Moquin, B. Zhang, P. Acharya, I. S. Georgiev, H. R. Altae-Tran, G.-Y. Chuang, M. G. Joyce, Y. D. Kwon, N. S. Longo, M. K. Louder, T. Luongo, K. McKee, C. A. Schramm, J. Skinner, Y. Yang, Z. Yang, Z. Zhang, A. Zheng, M. Bonsignori, B. F. Haynes, J. F. Scheid, M. C. Nussenzweig, M. Simek, D. R. Burton, W. C. Koff; NISC Comparative Sequencing Program, J. C. Mullikin, M. Connors, L. Shapiro, G. J. Nabel, J. R. Mascola, P. D. Kwong, Multidonor analysis reveals structural elements, genetic determinants, and maturation pathway for HIV-1 neutralization by VRC01-class antibodies. *Immunity* **39**, 245–258 (2013).
61. J. Zhu, S. O'Dell, G. Ofek, M. Pancera, X. Wu, B. Zhang, Z. Zhang; NISC Comparative Sequencing Program, J. C. Mullikin, M. Simek, D. R. Burton, W. C. Koff, L. Shapiro, J. R. Mascola, P. D. Kwong, Somatic populations of PGT135–137 HIV-1-neutralizing antibodies identified by 454 pyrosequencing and bioinformatics. *Front. Microbiol.* **3**, 315 (2012).
62. J. Zhu, G. Ofek, Y. Yang, B. Zhang, M. K. Louder, G. Lu, K. McKee, M. Pancera, J. Skinner, Z. Zhang, R. Parks, J. Eudailey, K. E. Lloyd, J. Blinn, S. M. Alam, B. F. Haynes, M. Simek, D. R. Burton, W. C. Koff; NISC Comparative Sequencing Program, J. C. Mullikin, J. R. Mascola, L. Shapiro, P. D. Kwong, Mining the antibodyome for HIV-1–neutralizing antibodies with next-generation sequencing and phylogenetic pairing of heavy/light chains. *Proc. Natl. Acad. Sci. U.S.A.* **110**, 6470–6475 (2013).
63. J. Zhu, X. Wu, B. Zhang, K. McKee, S. O'Dell, C. Soto, T. Zhou, J. P. Casazza; NISC Comparative Sequencing Program, J. C. Mullikin, P. D. Kwong, J. R. Mascola, L. Shapiro, De novo identification of VRC01 class HIV-1–neutralizing antibodies by next-generation sequencing of B-cell transcripts. *Proc. Natl. Acad. Sci. U.S.A.* **110**, E4088–E4097 (2013).
64. L. He, X. Lin, N. de Val, K. L. Saye-Francisco, C. J. Mann, R. Augst, C. D. Morris, P. Azadnia, B. Zhou, D. Sok, G. Ozorowski, A. B. Ward, D. R. Burton, J. Zhu, Hidden lineage complexity of glycan-dependent HIV-1 broadly neutralizing antibodies uncovered by digital panning and native-like gp140 trimer. *Front. Immunol.* **8**, 1025 (2017).
65. E. Krissinel, K. Henrick, Inference of macromolecular assemblies from crystalline state. *J. Mol. Biol.* **372**, 774–797 (2007).
66. I. W. Davis, A. Leaver-Fay, V. B. Chen, J. N. Block, G. J. Kapral, X. Wang, L. W. Murray, W. B. Arendall III, J. Snoeyink, J. S. Richardson, D. C. Richardson, MolProbity: All-atom contacts and structure validation for proteins and nucleic acids. *Nucleic Acids Res.* **35**, W375–W383 (2007).
67. R. A. Laskowski, M. B. Swindells, LigPlot+: Multiple ligand-protein interaction diagrams for drug discovery. *J. Chem. Inf. Model.* **51**, 2778–2786 (2011).
68. A. C. Martin, Accessing the Kabat antibody sequence database by computer. *Proteins* **25**, 130–133 (1996).

Acknowledgments: We thank R. Stanfield, X. Dai, and M. Elsliger for crystallographic and computational support; H. Tien in the Wilson lab for automated crystal screening; K. Cogburn, A. Honda, and K. Jackson for HCV donor sample analysis; and J. Ball for the UKN HCV constructs. **Funding:** This work was funded in part by NIH grants R01AI079031 (to M.L.), R01AI123365 and R01AI106005 (to M.L. and I.A.W.), U19AI123861 (to M.L. and J.Z.), U01AI131314 (to G.M.L.), and R01AI129698 (to J.Z.); the HIV Vaccine Research and Design (HIVRAD) program P01AI124337 (to J.Z.); the Danish Council for Independent Research DFF-4004-00598 (to J.B.); the Novo Nordisk Foundation NNF14OC001253 (to J.B.); and the Candys Foundation (to J.P., E.A., and J.B.). NBDS at TSRI was supported by the Clinical Translational Science Award (CTSA) grant UL1 TR001114. X-ray datasets were collected at the APS beamline 23ID-B (GM/CA CAT) and SSRL beamline 12-2. The use of the APS was supported by the U.S. Department of Energy (DOE), Basic Energy Sciences, Office of Science, under contract DE-AC02-06CH11357. The use of the SSRL Structural Molecular Biology Program was supported by the DOE Office of Biological and Environmental Research and by the NIH NIGMS (including P41GM103393) and the National Center for Research Resources (P41RR001209).
Author contributions: N.T., J.Z., I.A.W., and M.L. designed the project. N.T., E.G., and Y.H. expressed and purified the E2 proteins and mAbs. N.T. and L.K. determined and analyzed the x-ray structures. N.T., S.C., and E.G. determined K_Ds and assessed binding. J.Z. and L.H.

performed the NGS. J.P., E.A., and J.B. performed the HCVcc neutralization assays. G.M.L. provided the clinical samples and discussion, and N.T., J.B., J.Z., I.A.W., and M.L. wrote the manuscript with support from all the other authors. **Competing interests:** The authors declare that they have no competing interests. **Data and materials availability:** All data and code to understand and assess the conclusions of this research are available in the main text, Supplementary Materials, and the PDB (accession codes 6BKB, 6BKC, and 6BKD). Additional data related to this paper may be requested from the authors. This is manuscript 29614 from The Scripps Research Institute.

Submitted 22 August 2018
Accepted 27 November 2018
Published 2 January 2019
10.1126/sciadv.aav1882

Citation: N. Tzarum, E. Giang, L. Kong, L. He, J. Prentoe, E. Augestad, Y. Hua, S. Castillo, G. M. Lauer, J. Bukh, J. Zhu, I. A. Wilson, M. Law, Genetic and structural insights into broad neutralization of hepatitis C virus by human V_H1-69 antibodies. *Sci. Adv.* **5**, eaav1882 (2019).

ScienceAdvances

Genetic and structural insights into broad neutralization of hepatitis C virus by human V_H1-69 antibodies

Netanel Tzarum, Erick Giang, Leopold Kong, Linling He, Jannick Prentoe, Elias Augestad, Yuanzi Hua, Shaun Castillo, Georg M. Lauer, Jens Bukh, Jiang Zhu, Ian A. Wilson and Mansun Law

Sci Adv **5** (1), eaav1882.
DOI: 10.1126/sciadv.aav1882